Synthesis and structure–property relationships of donor/acceptor-functionalized bis(dehydrobenzo[18]annuleno)benzenes†

Eric L. Spitler and Michael M. Haley*

Received 17th January 2008, Accepted 22nd February 2008
First published as an Advance Article on the web 17th March 2008
DOI: 10.1039/b800875b

Seven new bis(dehydrobenzo[18]annuleno)benzenes (bis[18]DBAs) **1–7** functionalized with electron-donating dibutylamino groups and/or accepting nitro groups at various positions along the peripheries of the chromophores have been prepared. The effects of varying the donor/acceptor charge transfer pathways, chromophore lengths and molecular symmetries upon the optical band gaps are studied using UV–visible spectroscopy, and structure–property correlations are identified. It is found that bis[18]DBAs possessing donor–π–donor and acceptor–π–acceptor pathways exhibit the smallest band gaps, especially when an acceptor–π–acceptor pathway is situated along the longest chromophore length in the molecule. The all-donor species **1** is also found to exhibit efficient fluorescence with dramatic solvatochromism. The results may have value to the rational design of future NLO/TPA device components.

Introduction

The last decade has seen a dramatic expansion in the study of a special class of carbon-rich conjugated macrocycles, dehydrobenzoannulenes (DBAs),[1] due in part to their demonstrated unique optical, electronic and materials properties.[2] The increasing synthetic accessibility of desired molecular topologies and their site-specific functionalization allows these planar phenyl–acetylene macrocycles to display a host of intriguing characteristics, including enhanced π-orbital overlap, intermolecular π-stacking, and highly tunable dipoles and symmetries.[3] They thus possess potential in a wide array of applications such as fluorimetric sensing, organic electronics, organopolymers, and nonlinear optical (NLO) device components.[4] Large DBA assemblies have been shown to approximate the expected properties of theoretical all-carbon networks graphyne and graphdiyne,[5] and to serve as precursors for ordered nanomaterials.[6]

We have previously reported that DBA macrocycles and closely related phenyl–acetylene model systems functionalized with electron-donating and/or electron-accepting groups in a site-specific manner (*e.g.* Fig. 1) induce varying degrees of intramolecular charge transfer (ICT).[2a–d,7] We have also shown that the maximal low-energy two-photon absorption (TPA) cross-section, a key parameter in third-order NLO materials, of a particular DBA structure is often closely correlated to its ICT optical band gap in the steady-state one-photon absorption spectrum.[8] Thus, we have sought to elucidate structure–property relationships in donor/acceptor-functionalized DBAs for the design of customized NLO materials that also possess high molar extinction coefficients. We have demonstrated that while chromophore length affects optical band gap for these systems (which for our purposes is here taken simply as the energy corresponding to the longest wavelength λ_{max} in the absorption spectra), the *number* of chromophores (defined here as a linear conjugated pathway) affects the extinction coefficient.[2a,5] To that end, we now present a series of two-dimensional conjugated quadrupolar bis(dehydrobenzo[18]annuleno)benzenes (**1–7**, Fig. 2) functionalized with donor and acceptor groups at their peripheries. It is hoped that probing the photophysical effects of small variations in functional group orientation and conjugated charge transfer pathway topology will lead to an improved understanding of structure–property relationships, with ultimate application toward the rational design of the next generation of organic electronics.

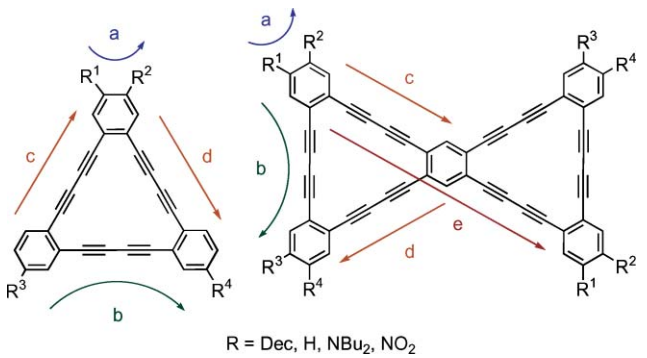

Fig. 1 Previously studied mono[18]DBAs with various conjugated pathways a–d and target bis[18]DBAs with conjugated pathways a–e.

BisDBAs **1–7** represent an expansion of our previous work on donor/acceptor-functionalized mono[18]DBAs.[2a,b] The fusion of two chromophore units into one molecule is expected to lead to similar optical band gaps in the absorption spectrum, but with higher molar extinction coefficients. Of the six target molecules, **2** and **6** are the only two belonging to an acentric point group and posses a net dipole. Furthermore, **1** is an all-donor analogue, and is believed to primarily exhibit non-ICT π–π* excitations (although a certain degree of weak charge transport from the donor nitrogens into the alkyne network is likely).[2c] These molecules thus represent

Department of Chemistry and Materials Science Institute, 1253 University of Oregon, Eugene, Oregon 97403-1253, USA. E-mail: haley@uoregon.edu; Fax: +1-541-346-0487; Tel: +1-541-346-0456

† Electronic supplementary information (ESI) available: Experimental details for synthesis of **2–6** and ^{1}H NMR spectra for all new compounds. See DOI: 10.1039/b800875b

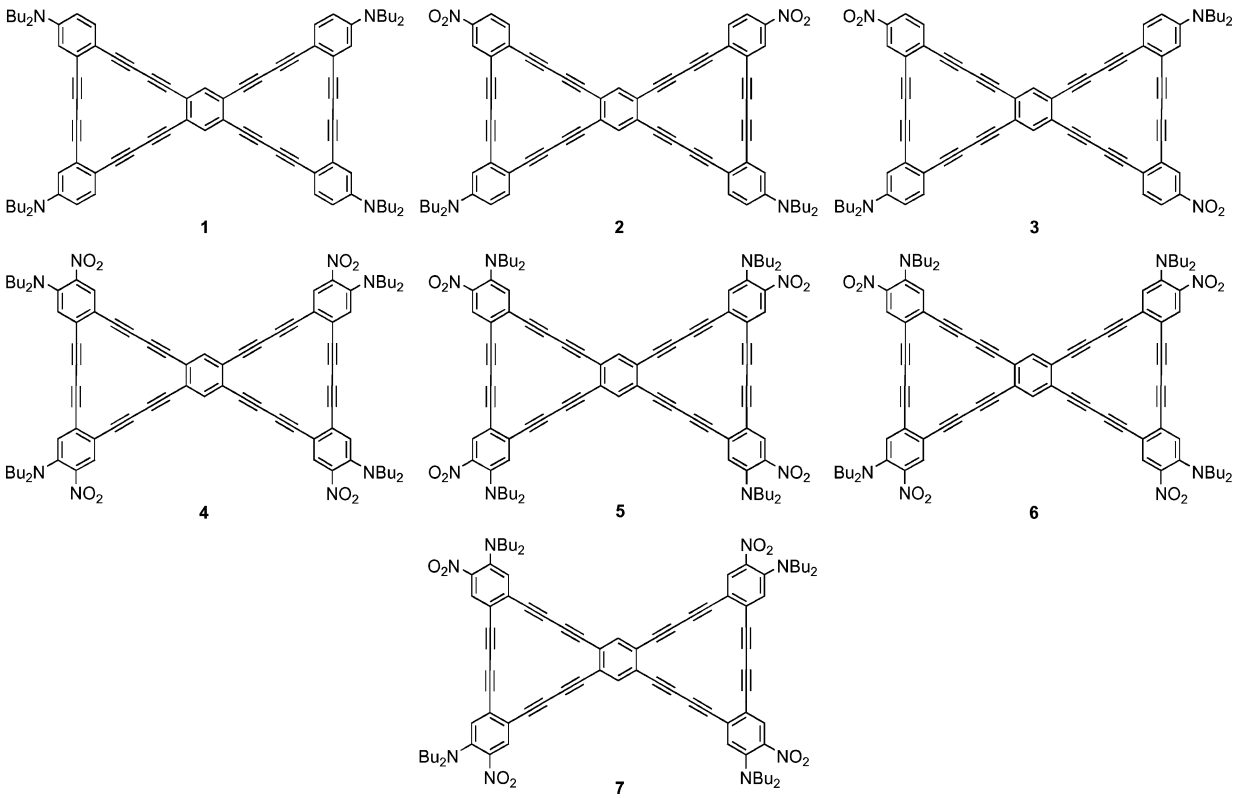

Fig. 2 Bis(dehydrobenzo[18]annuleno)benzenes **1–7**, the synthetic targets of this study.

good targets for comparison to quadrupolar bis[18]DBAs **3–5** and **7**.

Results and discussion

Synthesis

Synthesis of **1–7** is accomplished using a highly modular approach based on successive Pd-catalyzed Sonogashira cross-coupling reactions. Known donor/acceptor segments **8–11**[2a,b] (Fig. 3) can be appended to 1,2,4,5-tetraiodobenzene (*e.g.* Scheme 1) or an appropriate isomer of dibromodiiodobenzene (*e.g.* Scheme 2) using our selective *in situ* desilylation/cross-coupling protocol. Undesired homocoupling of the alkyne segments can be minimized to varying degrees of success by slowly injecting a solution of the triyne into the reaction mixture over a period of 8–12 h. Further desilylation followed by an oxidative intramolecular

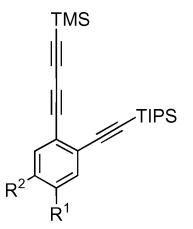

8 $R^1 = NBu_2$, $R^2 = H$
9 $R^1 = NO_2$, $R^2 = H$
10 $R^1 = NBu_2$, $R^2 = NO_2$
11 $R^1 = NO_2$, $R^2 = NBu_2$

Fig. 3 Differentially silylated donor/acceptor alkyne segments **8–11**.

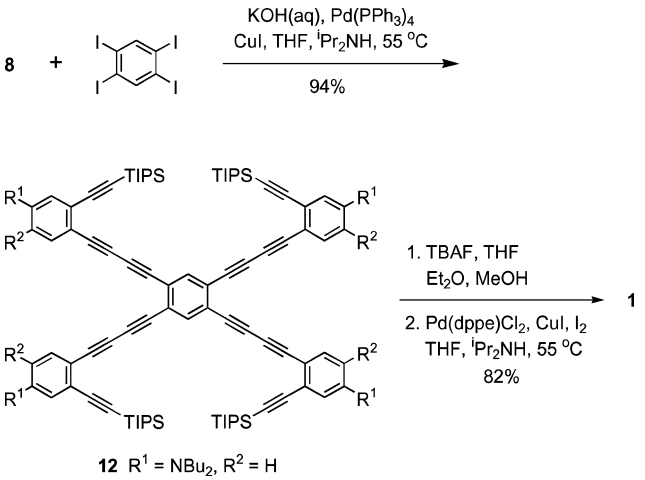

Scheme 1 Representative synthesis of **1**.

homocoupling under Pd-catalyzed oxidative conditions furnishes the corresponding bis[18]DBA in a wide range of yields (Table 1). The variation in isolated yield is likely due to a significant degree of intermolecular oligomerization. Certain topologies (**2** and **3**) have proven unstable, and rapidly decompose in solution. Consequently, only small amounts of these isomers could be prepared. This behaviour was also observed in several bis[14]- and bis[15]DBAs possessing similar donor/acceptor topologies (to such an extent that the 14-membered analogue of **3** could not be isolated at all), and is attributed to an uncontrolled topochemical 1,3-diacetylene polymerization promoted by strong intermolecular self-association and π-stacking (*vide infra*). The extreme

Table 1 Yields for alkyne segment couplings and cyclization to afford DBAs **1–7**

Entry	Arene	1st coupled segment (product, yield)	2nd coupled segment (product, yield)	DBA (yield)
1	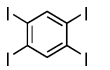	**8** (**12**, 94%)	—	**1** (82%)
2		**10** (**15**, 70%)	—	**4** (60%)
3		**11** (**16**, 92%)	—	**5** (49%)
4	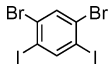	**9** (**17**, 86%)	**8** (**18**, 18%)	**2** (10%)
5		**11** (**19**, 78%)	**10** (**20**, 21%)	**6** (19%)
6	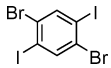	**9** (**21**, 71%)	**8** (**22**, 24%)	**3** (9%)
7		**11** (**13**, 87%)	**10** (**14**, 63%)	**7** (66%)

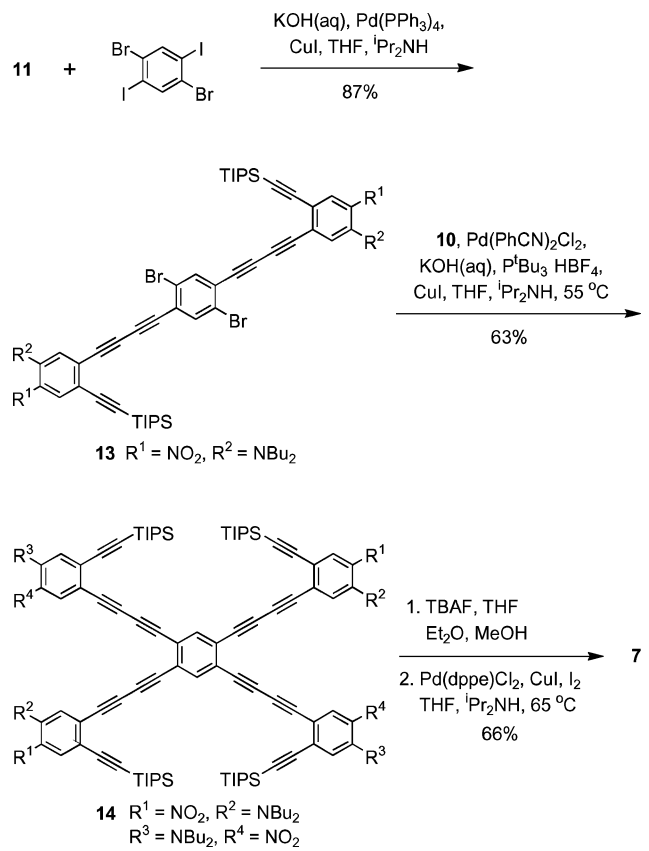

Scheme 2 Representative synthesis of **7**.

insolubility of **2** and **3** also precludes extensive chromatographic purification; trituration of the crude product with THF was found to be the only viable alternative. With these limitations in mind, **4–7** were assembled specifically to increase the number of donor/acceptor pathways and to avoid the strong polarization that leads to this degradative polymerization. The additional dibutylamino groups also greatly increase solubility. Due to anticipated synthetic and solubility issues, an all-acceptor analogue was not pursued. DBAs **4–7** are both soluble and stable in CD_2Cl_2 and $CDCl_3$, and do not undergo decomposition even when left in solution for several days.

Electronic absorption spectra

The UV–visible absorption spectra of **1–7** are given in Fig. 4. All compounds display longest-wavelength absorption maxima between 450 and 520 nm (Table 2). Except for tetra-donor **1**, all contain strong donor/acceptor functionalization.

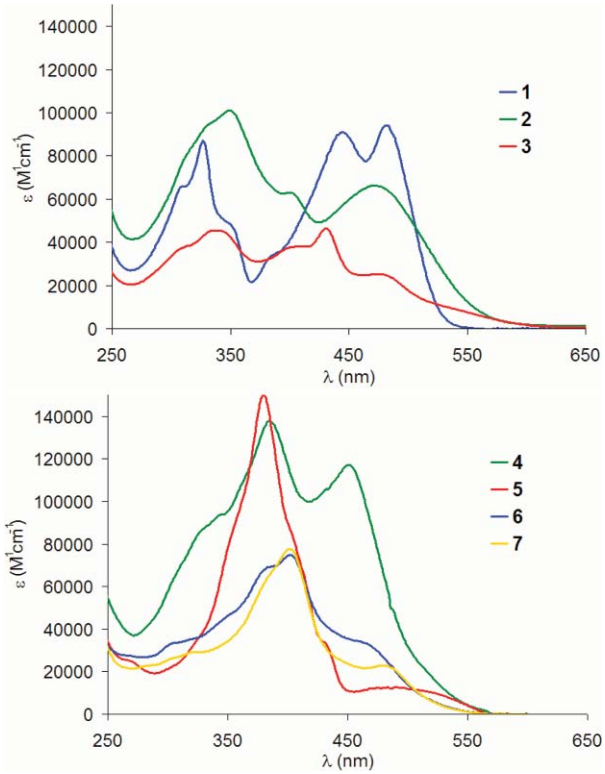

Fig. 4 Electronic absorption spectra of DBAs **1–3** (top) and **4–7** (bottom) in CH_2Cl_2 at *ca.* 10–25 μM concentrations.

Frontier molecular orbital (FMO) plots of these types of systems consistently predict strong localization of the HOMO on the donor-functionalized alkyne chromophore segments and the LUMO on the acceptor segments, implying intramolecular charge transfer as the lowest energy transition.[2c,d,7a] The low intensity, broadened peaks in this region for **2–7**, often accompanied by bathochromic shifts relative to **1**, are indicative of ICT behaviour and are consistent with our previous DBA studies.

Table 2 Lowest energy absorptions in **1–7**

DBA	Longest wavelength λ_{max}/nm (ε/M^{-1} cm^{-1})	Approximate λ_{cutoff}/nm[a]
1	481 (94 000)	557
2	471 (66 200)	604
3	517[b] (12 500)	614
4	451[c] (117 100)	578
5	490 (12 700)	575
6	456[b] (34 600)	568
7	480 (22 900)	564

[a] Cutoffs defined as the wavelength after the lowest energy λ_{max} where there is less than a 200 M^{-1} cm^{-1} variation over a 5 nm range. [b] Approximate λ_{max}, as band is only a shoulder. [c] There is likely a low-intensity ICT transition manifested at *ca.* 500 nm, but the overlap with the next highest band makes it difficult to determine its λ_{max}.

In all compounds, conversion from the acyclic precursors to the corresponding bisDBA results in a bathochromic shift in the absorption spectra (example spectra, Fig. 5). This is likely due to an enhanced conjugation effect from the enforced planarization. It is notable that for DBAs **1** and **4**, with donor groups situated along the longest linear chromophore path, cyclization causes an increase in molar extinction coefficient in the longest wavelength band in addition to a bathochromic shift, whereas in the other systems a corresponding decrease is seen. This is presumably due to enhanced ICT and delocalization in the planarized macrocycles.

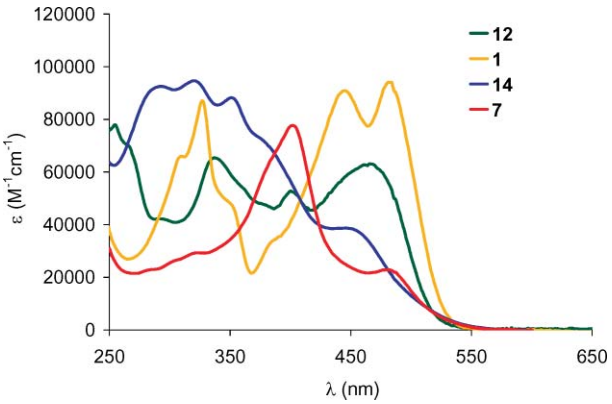

Fig. 5 Electronic absorption spectra of acyclic precursors **12** and **14** and their respective DBAs **1** and **7**.

Comparing two-donor/two-acceptor DBAs **2** and **3** to tetradonor **1**, we see a significant broadening of the corresponding bands, with absorption cutoffs extending past 600 nm. In the case of **3**, the lowest discernible band exists as a shoulder beginning near 517 nm, indicating a narrowed optical band gap relative to **1**. Interestingly, the ICT band in **2** is slightly blue-shifted from **1**. This was initially a surprising result, since **2** contains two long, linear conjugated pathways from the donor groups to the acceptor groups; one might intuitively expect such a topology to exhibit a significantly narrowed band gap. This result is consistent, however, with previous observations by Meier *et al.*[9] who also noted hypsochromic shifts in the absorption spectra of certain extended chromophores upon strong donor/acceptor functionalization. In those cases, the nearly complete lack of calculated Franck–Condon overlap actually resulted in predominantly non-HOMO–LUMO transitions as the dominant absorptions. Furthermore, Moonen and Diederich have observed a lack of correlation between optical band gap and conjugated pathway efficiency for certain donor/acceptor cyanoethynylethene systems,[10] finding instead that quadrupolar compounds with bent donor/acceptor pathways (analogous to pathway *c*–*d* in Fig. 1) often display smaller band gaps than corresponding dipolar analogues with linear pathways (path *e* in Fig. 1). Our own systematic structure–property studies involving isomeric permutations of particular acyclic donor/acceptor motifs have confirmed this phenomenon.[2c,7] Note that **3** is quadrupolar rather than dipolar, and exhibits the smallest band gap of the DBAs presented here. This property could potentially have consequences for the future design of organic NLO materials, particularly those that rely on good two-photon absorption (TPA) parameters. We have shown that systems with either symmetric multi-chromophore units or strong donor/acceptor-functionalization can display particularly high TPA cross-sections.[2f,8] The DBAs presented here, which possess both qualities, are expected to follow suit.

The absorption spectra of the four-donor/four-acceptor DBAs **4**–**7** provide further insight into structural effects on band gap. Each of these compounds contains four donor groups and four acceptor groups; only their orientation with respect to the DBA skeleton varies. Here only **6** possesses a net dipole, while all the others are quadrupolar, thus allowing us to investigate only the effects of conjugated pathway topology on the band gap. It is interesting to note that **4**–**7** display absorption cutoffs at very similar wavelengths. The most striking feature, however, is the high molar extinction coefficient in **4**, whose spectrum somewhat resembles tetradonor **1**. This is not surprising, since the four donor groups lie along the longest conjugated chromophores as in **1**, with the acceptor groups along the bridging diacetylenes. A close look at the spectrum of **4** reveals a possible lower energy ICT transition around 500 nm, similar to those of **5**–**7**, but the next highest band overlaps too greatly for even speculative deconvolution. **5**–**7** display more characteristic low-intensity ICT bands red-shifted from **4**, with **5** possessing the smallest band gap. DBA **5** most resembles a 'tetraacceptor' system, with acceptor groups along the longest conjugated pathway, and donors along the diacetylene bridges. DBAs **6** and **7** lie in between these two extremes. In these cases, the dipolar DBA **6**, which contains only linear donor–π–acceptor pathways, is only slightly red-shifted from **4**, while **7** (with only two linear ICT pathways) and **5** (with no linear ICT pathways) are more red-shifted. Thus, we are led to the conclusion that for these systems, a supposedly 'efficient' linear donor–π–acceptor conjugated chromophore does not lead to the lowest energy charge transfer transition.

Comparing all the spectra of **1**–**7**, we can note that placing like groups along a longest chromophore (donor–π–donor or acceptor–π–acceptor) results in the smallest band gaps, with acceptor–π–acceptor arrangements being particularly effective. This makes sense when considering the likely FMO localizations (which were not computed for these systems here, but for which there is extensive precedent from our earlier studies[2c–e,7a]): rather than exhibiting the behaviour of a donor atom transferring electron density to an acceptor atom, the spectra imply a transition from an electron-rich chromophore to an electron-poor chromophore, wherein two directly conjugated donor groups contribute to generate the former, and two acceptor groups contribute to the latter. The band gap is thus more dependent on the length of the linear chromophores, and hence is smaller for the quadrupolar systems than for the dipolar ones. This 'synergistic cooperation' was also observed for our previously-reported mono[18]DBAs:[2a] the smallest band gaps occurred when a donor was conjugated to a donor and an acceptor to an acceptor. Linear donor/acceptor pathways exhibited larger band gaps. In those cases, however, the necessary asymmetry of most of the DBAs could lead to potential skewing from dissimilar net dipole effects which are not present in most of the bis[18]DBAs presented here. Finally, our most bathochromic systems here, **3** and **5**, display charge transfer bands with molar extinction coefficients roughly double those of analogous mono[18]DBAs, but in the same 490–530 nm region. In donor-functionalized systems, the bisDBAs display both higher extinction coefficients from fusion of a second annulenic unit *and* longer wavelength absorptions from extension of the chromophore lengths.

Electronic emission spectra

Many of the DBAs and donor/acceptor systems we have presented in the past exhibit efficient fluorescence.[2c,d,5,7] Small structural variations of the conjugated pathways (*e.g.* chromophore topology, polarization, planarity, donor or acceptor strength, protonation or metal ion complexation ability) can fine-tune both emission wavelength and quantum yield. In nitro-functionalized systems, however, the high internal conversion rate caused by mixing of vibronic states as well as solvent interaction effectively quenches fluorescence.[2c,7b] The only highly emissive DBA presented here is therefore tetradonor **1** (Φ_f = 0.34 in CH_2Cl_2). The long, electron-rich conjugated pathways and the lack of a net dipole likely result in an excited state that is highly polarized relative to the ground state. The photophysical manifestation of this is a dramatic degree of fluorescence solvatochromism (Fig. 6), with emission maxima ranging from 486 nm in hexane to 587 nm in acetone. The absorption spectra, by contrast (Table 3), display only slight solvent dependence, implying that the effect is enhanced by relaxation to increasingly low-lying vibrational levels of the S_1 state after initial excitation (note the gradual loss of vibronic fine structure in Fig. 6 as solvent polarity increases). In contrast, DBA **4**, which also has its donor groups along the longest chromophores but also acceptors along the diacetylene bridges, is only slightly fluorescent (quantum yield < 0.05), with much less solvent dependence (Fig. 7). DBAs **2**, **3**, and **5–7** do not fluoresce at all. No concentration dependence was noted in either absorption or emission spectra for any compound.

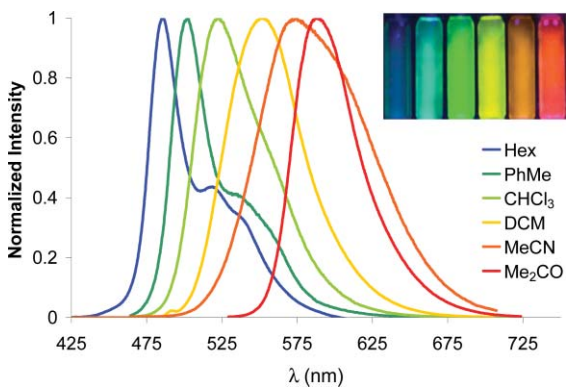

Fig. 6 Normalized electronic emission spectra of **1** in hexanes (Hex), toluene (PhMe), chloroform ($CHCl_3$), dichloromethane (DCM), acetonitrile (MeCN), and acetone (Me_2CO) at *ca.* 10–25 μM concentrations. Excitation at 365 nm. Inset: photographs of solutions of **1** in corresponding solvents (left to right) under illumination by high-intensity 365 nm lamp.

Table 3 Lowest energy absorption and emission wavelengths of **1** in various solvents

Solvent	Absorption λ_{max}/nm	Emission λ_{max}/nm
Hexanes	466	486
Toluene	471	502
Chloroform	478	522
Dichloromethane	481	551
Acetonitrile	482	575
Acetone	479	587

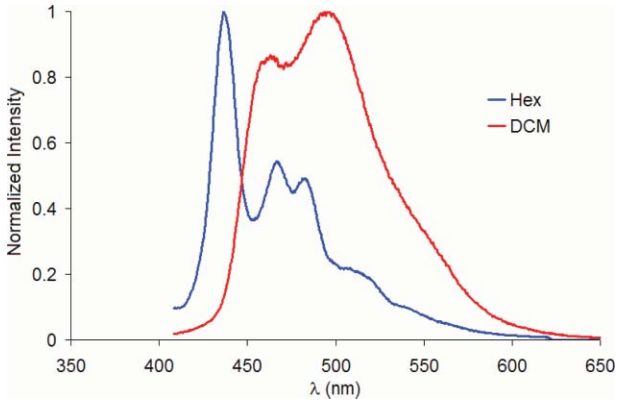

Fig. 7 Normalized electronic emission spectra of DBA **4** in hexanes (Hex) and dichloromethane (DCM). Excitation at 381 and 386 nm, respectively.

Self-association

Our previously reported bis[14]- and bis[15]DBAs (*e.g.* **23** and **24**, Fig. 8),[2c] also functionalized with dibutylamino and nitro groups, displayed a significant degree of intermolecular self-association in solution, presumably due to π-stacking enhanced by attraction between donor and acceptor groups between molecules. The aggregation manifested upfield shifts of the ^{1}H-NMR signals of the aromatic protons with increasing concentration. It was confirmed that the monomer–dimer equilibrium is the dominant process in these systems, and hence dimerization constants could be calculated from the concentration-dependent chemical shifts. This effect was not observed in DBAs **1** or **4–7**, or in equimolar mixtures of **4** and **5** (which could theoretically form dimer aggregates when respective donor and acceptor groups from each molecule are π-stacked). It is believed that the *ortho* relationship between the alkylamino and nitro groups on each arene ring can prevent strong polarization (dipolar or quadrupolar) and effectively 'cancel out' any long-range intermolecular attraction. Also, aggregation may be prevented in these cases by the fact that *ortho* substitution will result in one or both of the substituents not being co-planar with the arene ring. This can create 'thickness' in the molecule that inhibits stacking interactions. Tetradonor **1** possesses no acceptor groups to enhance π-stacking *via* intermolecular attraction.

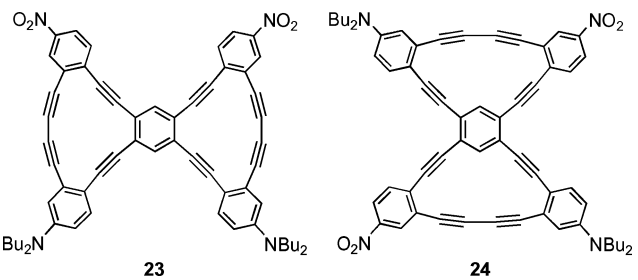

Fig. 8 Examples of previously reported bis[14]- and bis[15]DBAs that display self-association in solution.

DBA **2** underwent rapid degradation in $CDCl_3$ solution, so concentration-dependent experiments could not be conducted. DBA **3**, however, remained stable long enough for several concentration-dependence data points to be collected (Fig. 9). The protons residing on the donor and acceptor arene rings experienced the greatest degree of upfield shifts, and the central

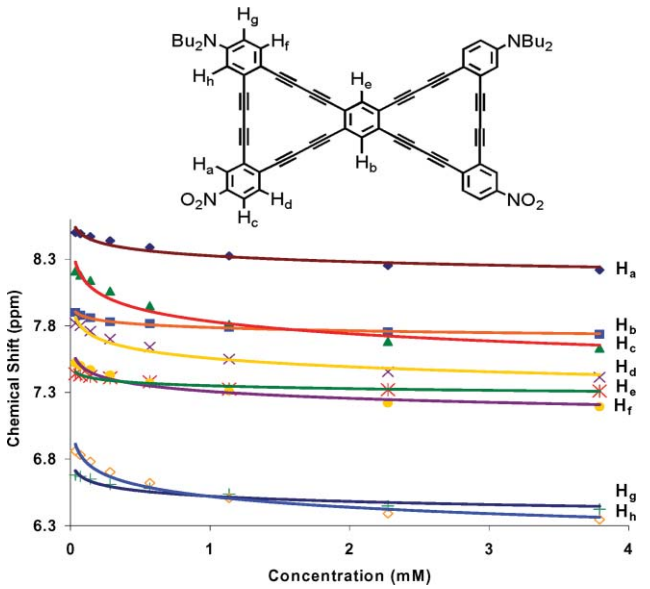

Fig. 9 Concentration-dependent chemical shifts of the aromatic protons of bis[18]DBA **3** in $CDCl_3$ at 20 °C.

arene ring protons experienced the least, indicating the greatest degree of change in the shielding environment where the donors of one molecule interact with the acceptors of another, and *vice versa*. The gradual upfield shifts were fitted to curves using the HypNMR program[11] from which a dimerization constant of 515 ± 31 M^{-1} was extracted. This value is only slightly larger than for the smaller analogous DBA **23** (326 ± 51 M^{-1}), and may be due to more efficient stacking due to increased π-orbital overlap in the strain-free bis[18]DBA, as well as due to the increased total number of π–π interactions.

Conclusions

Bis[18]DBAs **1–7** represent an interesting systematic investigation into the effects of conjugation pathway topology, chromophore length, and symmetry on the optical band gaps of carbon-rich intramolecular charge transfer systems. We have demonstrated that quadrupolar chromophores with linear donor–π–donor and acceptor–π–acceptor pathways can exhibit narrowed band gaps *versus* donor–π–acceptor analogues, and comparison to our earlier mono[18]DBAs shows that, while extending the length of a donor-functionalized system results in absorption red shifts, increasing the number of chromophore units in the system causes an increase in molar extinction coefficient. Our studies also support observations in other systems that strong donor/acceptor functionalization of an extended chromophore can actually lead to increased band gaps due to lack of Franck–Condon overlap of segment-isolated FMOs.[9,10] It has been shown in the past that highly conjugated organic molecules often exhibit high TPA cross-sections, especially when possessing either high symmetry or donor/acceptor functionalization.[2e,f,8] The systems presented here satisfy both conditions, so it is expected that they will display particularly favorable results, and we hope to report the outcome of these experiments in the near future.

Experimental

General methods

^1H- and ^{13}C-NMR spectra were recorded in $CDCl_3$ using a Varian Inova 300 (^1H: 299.94 MHz, ^{13}C: 75.43 MHz) or 500 (^1H: 500.10 MHz, ^{13}C: 125.75 MHz) spectrometer. Chemical shifts (δ) are expressed in ppm relative to the residual chloroform (^1H: 7.26 ppm, ^{13}C: 77.0 ppm) reference. Coupling constants are expressed in Hertz. Melting points were recorded on a Melt-Temp II melting point apparatus in open-end capillary tubes or on a TA Instruments 2920 DSC and are uncorrected. IR spectra were recorded using a Nicolet Magna FTIR 550 spectrometer. UV–vis spectra were recorded on an HP 8453 UV–vis spectrophotometer. Fluorescence data were recorded on a Hitachi F-4500 fluorescence spectrophotometer. Mass spectra were recorded on an Agilent 1100 SL Series LC/MSD spectrometer. THF and Et_2O were distilled from Na–benzophenone under N_2. All other chemicals were of reagent quality and used as obtained from manufacturers. Column flash chromatography was performed using N_2 or air pressure on Sorbent Technologies silica gel (230–450 mesh). Pre-coated silica gel plates (Sorbent Technologies, 200 × 200 × 0.50 mm) were used for analytical thin layer chromatography. Eluting solvents were reagent quality and used as obtained from the manufacturers. Reactions were carried out in an inert atmosphere (dry Ar) when necessary. All deprotected terminal alkynes were used directly without further purification. Syntheses of segments **8–11** have been described previously.[2a,b]

General alkyne coupling procedure A. Alkyne segment **8**, **10**, or **11** (5.0 equiv.) and 1,2,4,5-tetraiodobenzene (1 equiv.) were dissolved in $^iPr_2NH$–THF (1 : 1, 0.003 M) and the solution was purged for 30 min with bubbling Ar. $PdCl_2(PPh_3)_2$ (0.03 equiv. per transformation), CuI (0.06 equiv. per transformation) and aqueous KOH (5 equiv. per transformation) were added and the solution was purged for another 20 min. The reaction mixture was stirred at 55 °C for 24–48 h under an Ar atmosphere until complete by TLC. The mixture was then concentrated, rediluted with hexanes, and filtered through a pad of silica gel. The solvent was removed *in vacuo* and the crude material was used without further purification.

General alkyne coupling procedure B. Acceptor segment **9** or **11** (2.5 equiv.) and the appropriate isomer of dibromodiiodobenzene (1 equiv.) were dissolved in $^iPr_2NH$–THF (1 : 1, 0.003 M) and the solution was purged for 30 min with bubbling Ar. $PdCl_2(PPh_3)_2$ (0.03 equiv. per transformation), CuI (0.06 equiv. per transformation) and aqueous K_2CO_3 (5 equiv. per transformation) were added and the solution was purged for another 20 min. The reaction mixture was stirred at room temperature for 24–48 h under an Ar atmosphere until complete by TLC. The mixture was then concentrated, rediluted with hexanes, and filtered through a pad of silica gel. The solvent was removed *in vacuo* and the crude material was used without further purification.

General alkyne coupling procedure C. Acceptor-functionalized tetrayne **13**, **17**, **19** or **21**, and aqueous KOH (5 equiv. per transformation) were dissolved in $^iPr_2NH$–THF (3 : 2, 0.004 M) and the solution was purged for 30 min with bubbling Ar. $Pd(PhCN)_2Cl_2$ (0.03 equiv. per transformation), $P^tBu_3{\cdot}HBF_4$ (0.07 equiv. per transformation) and CuI (0.06 equiv. per transformation) were

added and the solution was purged for another 20 min under bubbling Ar. Donor segment **8** or **10** (2.5 equiv.) was dissolved in THF (0.04 M), the solution was purged for 30 min under bubbling Ar, and then injected *via* syringe pump into the stirred polyyne solution over 8 h at 55 °C under an Ar atmosphere. The reaction was stirred until complete by TLC. The mixture was then concentrated, rediluted with hexanes–CH_2Cl_2 (4 : 1), and filtered through a pad of silica gel. The solvent was removed *in vacuo*, and the crude material was purified by column chromatography.

General Pd-catalyzed cyclization procedure D. Annulene precycle was dissolved in THF, Et_2O and MeOH (2 : 1 : 0.01, 0.005 M) and Bu_4NF (TBAF, 1.0 M soln in THF, 10 equiv.) was added. The solution was stirred at room temperature until complete by TLC (typically <1 h). The reaction mixture was then concentrated, dissolved in Et_2O, and washed with H_2O (3 × 50 mL). The organic phase was collected, dried over $MgSO_4$, and filtered through a pad of silica gel eluting with hexanes. The solvent was removed *in vacuo* and the deprotected precycle was dissolved in THF (0.005 M). $PdCl_2$(dppe) (0.1 equiv. per transformation), CuI (0.2 equiv. per transformation), and I_2 (0.25 equiv. per transformation) were dissolved in $^iPr_2NH$–THF (3 : 2, ~0.5 L per mmol precycle). To this mixture, the deprotected precycle solution was injected *via* syringe pump over 40 h at 65 °C. The reaction mixture was stirred until complete by TLC, then concentrated, rediluted in hexanes–CH_2Cl_2 (3 : 1) and filtered through a pad of silica gel. The solvent was removed *in vacuo* and the product was triturated with hexanes.

*DBA precursor **12**.* Segment **8** (306 mg, 0.605 mmol) was cross-coupled to 1,2,4,5-tetraiodobenzene (78 mg, 0.134 mmol) at 55 °C using general alkyne coupling procedure A (12 h). The crude material was chromatographed on silica gel (4 : 1 hexanes–CH_2Cl_2) to give **12** (227 mg, 94%) as a dark red oil. λ_{max} (CH_2Cl_2)/nm 400 (log ε/dm^3 mol^{-1} cm^{-1}, 4.73), 466 (4.81). Em. λ_{max}/nm 551. Φ_f 0.18.[12] ν_{max} (NaCl)/cm^{-1} 2959, 2935, 2856, 2191, 2155, 1589, 1530, 1479, 1365, 1223, 1113. δ_H (300 MHz; $CDCl_3$; Me_4Si) 7.51 (2 H, s), 7.35 (4 H, d, *J* 9.0), 6.66 (4 H, d, *J* 2.7), 6.49 (4 H, dd, *J* 9.0, 2.7), 3.27 (16 H, t, *J* 7.5), 1.54 (16 H, quin, *J* 7.5), 1.34 (16 H, sext, *J* 7.2), 1.18 (84 H, s), 0.96 (24 H, t, *J* 7.2). δ_C (75 MHz; $CDCl_3$; Me_4Si) 148.30, 137.66, 134.58, 128.57, 125.49, 114.89, 111.72, 110.40, 105.84, 94.59, 85.37, 81.84, 78.87, 75.99, 50.78, 29.50, 20.48, 18.97, 14.16, 11.60. *m/z* (APCI) 1719 (M$^+$ − TIPS + THF, 66%), 1720 (M$^+$(^{13}C) − TIPS + THF, 100).

*Bis[18]DBA **1**.* Precursor **12** (136 mg, 0.075 mmol) was subjected to general Pd-catalyzed cyclization procedure D (40 h). The crude material was purified by filtration through a pad of silica gel followed by concentration *in vacuo* and trituration with hexanes to afford **1** (72 mg, 82%) as a brick red powder. Once purified, the product exhibited very poor solubility, thus precluding acquisition of ^{13}C-NMR data. Mp: 200–220 °C (dec). λ_{max} (CH_2Cl_2)/nm 445 (log ε/dm^3 mol^{-1} cm^{-1}, 4.96), 481 (4.98). Em. λ_{max}/nm 551. Φ_f 0.34.[12] ν_{max} (KBr)/cm^{-1} 2956, 2929, 2871, 2136, 1591, 1590, 1482, 1368, 1218, 1110. δ_H (300 MHz; $CDCl_3$; Me_4Si) 7.78 (2 H, s), 7.49 (4 H, d, *J* 8.7), 6.84 (4 H, s), 6.66 (4 H, d, *J* 11.4), 3.30 (16 H, t, *J* 6.9), 1.59 (16 H, m), 1.40 (16 H, sext, *J* 7.8), 0.99 (24 H, t, *J* 7.2). δ_H (300 MHz; THF-d_8; Me_4Si) 7.84 (2 H, s), 7.50 (4 H, d, *J* 9.0), 6.92 (4 H, s), 6.80 (4 H, d, *J* 9.0), 3.39 (16 H, t, *J* 7.8), 1.63 (16 H, m), 1.40 (16 H, sext, *J* 7.5), 0.99 (24 H, t, *J* 7.5).

*Acceptor-functionalized arene **13**.* Segment **11** (198 mg, 0.359 mmol) was cross-coupled to 1,4-dibromo-2,5-diiodobenzene (72 mg, 0.148 mmol) at rt for 16 h using general alkyne coupling procedure B. The crude material was chromatographed on silica gel (4 : 1 hexanes–CH_2Cl_2) to give **13** (153 mg, 87%) as a red oil. ν_{max} (KBr)/cm^{-1} 2958, 2937, 2860, 2150, 1652, 1591, 1540, 1506, 1472, 1457, 1338, 1277. δ_H (300 MHz; $CDCl_3$; Me_4Si) 7.82 (2 H, s), 7.72 (2 H, s), 7.20 (2 H, s), 3.12 (8 H, t, *J* 6.9 Hz), 1.53 (8 H, quin, *J* 7.5), 1.29 (8 H, sext, *J* 7.5), 1.15 (42 H, s), 0.88 (12 H, t, *J* 7.2). δ_C (75 MHz; $CDCl_3$; Me_4Si) 144.25, 140.92, 137.61, 130.59, 128.52, 126.35, 125.21, 124.54, 116.94, 102.96, 96.13, 81.84, 81.51, 80.07, 78.98, 51.96, 29.71, 20.29, 18.98, 14.06, 11.54. *m/z* (APCI) 1187 (M$^+$(^{79}Br), 42%), 1189 (MH$^+$(^{79}Br^{81}Br), 100), 1190 (MH$^+$(^{13}C2^{81}Br), 65).

*DBA precursor **14**.* Segment **10** (106 mg, 0.192 mmol) was cross-coupled to acceptor-functionalized arene **13** (106 mg, 0.089 mmol) at 55 °C using general alkyne coupling procedure C (10 h). The crude material was chromatographed on silica gel (4 : 1 hexanes–CH_2Cl_2) to give **14** (111 mg, 63%) as a dark red oil. λ_{max} (CH_2Cl_2)/nm 294 (log ε/dm^3 mol^{-1} cm^{-1}, 4.97), 322 (4.98), 353 (4.94), 445 (4.59). ν_{max} (NaCl)/cm^{-1} 2953, 2932, 2891, 2856, 2218, 2147, 1595, 1536, 1505, 1487, 1466, 1428, 1337, 1274. δ_H (300 MHz; $CDCl_3$; Me_4Si) 7.90 (2 H, s), 7.82 (2 H, s), 7.60 (2 H, s), 7.22 (2 H, s), 7.10 (2 H, s), 3.13 (16 H, m), 1.52 (16 H, m), 1.29 (16 H, m), 1.16 (42 H, s), 1.14 (42 H, s), 0.88 (24 H, m). δ_C (75 MHz; $CDCl_3$; Me_4Si) 145.32, 144.30, 140.91, 139.50, 138.01, 131.68, 131.62, 130.59, 128.79, 125.81, 125.55, 125.33, 124.11, 117.03, 113.25, 103.56, 102.98, 100.25, 99.87, 96.09, 82.71, 82.44, 81.63, 80.76, 80.29, 79.60, 78.86, 51.96, 51.76, 29.71, 20.26, 18.94, 14.02, 11.53.

*Bis[18]DBA **7**.* Precursor **14** (65 mg, 0.033 mmol) was subjected to general Pd-catalyzed cyclization procedure D (40 h). The crude material was purified by filtration through a pad of silica gel followed by concentration *in vacuo* and trituration with hexanes to afford **7** (29 mg, 66%) as a dark orange powder. Mp: 160–180 °C (dec). λ_{max} (CH_2Cl_2)/nm 403 (log ε/dm^3 mol^{-1} cm^{-1}, 4.89), 479 (4.36). ν_{max} (NaCl)/cm^{-1} 2955, 2924, 2868, 2213, 1651, 1592, 1535, 1479, 1431, 1370. δ_H (300 MHz; CD_2Cl_2; Me_4Si) 8.01 (2 H, s), 8.00 (2 H, s), 7.88 (2 H, s), 7.36 (2 H, s), 7.32 (2 H, s), 3.20 (16 H, m), 1.55 (16 H, m), 1.29 (16 H, m), 0.91 (24 H, m). δ_C (75 MHz; $CDCl_3$; Me_4Si) 145.09, 139.86, 139.75, 139.50, 137.46, 136.69, 131.72, 129.77, 129.41, 125.77, 125.25, 124.25, 124.06, 113.15, 113.03, 82.14, 81.92, 81.35, 81.27, 80.94, 80.78, 80.71, 80.19, 79.83, 79.41, 77.46, 77.41, 51.70, 29.71, 20.33, 14.05.

Acknowledgements

We thank the National Science Foundation (CHE-0718242) for financial support. E.L.S. acknowledges the NSF for an IGERT fellowship (DGE-0549503). We thank the laboratory of Prof. D. W. Johnson for use of the HypNMR program software.

Notes and references

1 (*a*) E. L. Spitler, C. A. Johnson and M. M. Haley, *Chem. Rev.*, 2006, **106**, 5344–5386; (*b*) J. A. Marsden, G. J. Palmer and M. M. Haley, *Eur. J. Org. Chem.*, 2003, 2355–2369.

2 (*a*) J. J. Pak, T. J. R. Weakley and M. M. Haley, *J. Am. Chem. Soc.*, 1999, **121**, 8182–8192; (*b*) A. Sarkar, J. J. Pak, G. W. Rayfield and M. M. Haley, *J. Mater. Chem.*, 2001, **11**, 2943–2945; (*c*) J. A. Marsden, J. J. Miller, L. D. Shirtcliff and M. M. Haley, *J. Am. Chem. Soc.*, 2005, **127**, 2464–2476; (*d*) E. L. Spitler, S. P. McClintock and M. M. Haley, *J. Org. Chem.*, 2007, **72**, 6692–6699; (*e*) S. Anand, O. Varnavski, J. A. Marsden,

M. M. Haley, H. B. Schlegel and T. Goodson, *J. Phys. Chem. A*, 2006, **110**, 1305–1318; (*f*) A. Sarkar, R. Guda, M. M. Haley and T. Goodson, *J. Am. Chem. Soc.*, 2006, **128**, 13972–13973.

3 C. S. Jones, M. J. O'Connor and M. M. Haley, in *Acetylene Chemistry–Chemistry, Biology, and Materials Science*, ed. F. Diederich, P. J. Stang and R. R. Tykwinski, Wiley-VCH, Weinheim, 2005, pp. 303–385.

4 (*a*) *Nonlinear Optics of Organic Molecules and Polymers*, ed. H. S. Nalwa and S. Miyata, CRC Press, Boca Raton, 1997; (*b*) *Electronic Materials: The Oligomer Approach*, ed. K. Müllen and G. Wegner, Wiley-VCH, Weinheim, 1998; (*c*) *Carbon-Rich Compounds: From Molecules to Materials*, ed. M. M. Haley and R. R. Tykwinski, Wiley-VCH, Weinheim, 2006; (*d*) *Organic Light Emitting Devices: Synthesis, Properties and Applications*, ed. K. Mullen and U. Scherf, Wiley-VCH, Weinheim, 2006; (*e*) *Functional Organic Materials*, ed. T. J. J. Müller and U. H. F. Bunz, Wiley-VCH, Weinheim, 2007.

5 (*a*) J. A. Marsden and M. M. Haley, *J. Org. Chem.*, 2005, **70**, 10213–10226; (*b*) C. A. Johnson, II, Y. Lu and M. M. Haley, *Org. Lett.*, 2007, **9**, 3725–3728.

6 (*a*) R. Boese, A. J. Matzger and K. P. C. Vollhardt, *J. Am. Chem. Soc.*, 1997, **119**, 2052–2053; (*b*) M. Laskoski, W. Steffen, J. G. M. Morton, M. D. Smith and U. H. F. Bunz, *J. Am. Chem. Soc.*, 2002, **124**, 13814–13817; (*c*) K. Tahara, S. Furukawa, H. Uji-i, T. Uchino, T. Ichikawa, J. Zhang, M. Sonoda, F. C. De Schryver, S. De Feyter and Y. Tobe, *J. Am. Chem. Soc.*, 2006, **128**, 16613–16625; (*d*) K. Tahara, C. A. Johnson II, T. Fujita, M. Sonoda, F. De Schryver, S. De Feyter, M. M. Haley and Y. Tobe, *Langmuir*, 2007, **23**, 10190–10197.

7 (*a*) E. L. Spitler, L. D. Shirtcliff and M. M. Haley, *J. Org. Chem.*, 2007, **72**, 86–96; (*b*) S. Samori, S. Tojo, M. Fujitsuka, E. L. Spitler, M. M. Haley and T. Majima, *J. Org. Chem.*, 2007, **72**, 2785–2793; (*c*) E. L. Spitler, J. M. Monson and M. M. Haley, *J. Org. Chem.*, 2008, **73**, 2211–2223.

8 A. Slepkov, F. A. Hegmann, R. R. Tykwinski, K. Kamada, K. Ohta, J. A. Marsden, E. L. Spitler, J. J. Miller and M. M. Haley, *Opt. Lett.*, 2006, **31**, 3315–3317.

9 H. Meier, B. Mühling and H. Kohlshorn, *Eur. J. Org. Chem.*, 2004, 1033–1042.

10 N. N. P. Moonen and F. Diederich, *Org. Biomol. Chem.*, 2004, **2**, 2263–2266.

11 (*a*) C. Frassineti, S. Ghelli, P. Gans, A. Sabatini, M. S. Moruzzi and A. Vacca, *Anal. Biochem.*, 1995, **231**, 374–382; (*b*) C. Frassineti, L. Alderighi, P. Gans, A. Sabatini, A. Vacca and S. Ghelli, *Anal. Bioanal. Chem.*, 2003, **376**, 1041–1052; (*c*) A. Vacca, C. Nativi, M. Cacciarini, R. Pergoli and S. Roelens, *J. Am. Chem. Soc.*, 2004, **126**, 16456–16465.

12 Quantum yields determined from steady-state spectra using the methods described in: H. V. Drushel, A. L. Sommers and R. C. Cox, *Anal. Chem.*, 1963, **35**, 2166–2172.

